Atmos. Meas. Tech., 8, 4785–4801, 2015
www.atmos-meas-tech.net/8/4785/2015/
doi:10.5194/amt-8-4785-2015

Atmospheric Measurement Techniques
Open Access
EGU

Assessing 5 years of GOSAT Proxy XCH_4 data and associated uncertainties

R. J. Parker[1,2], H. Boesch[1,2], K. Byckling[1], A. J. Webb[1], P. I. Palmer[3,4], L. Feng[3,4], P. Bergamaschi[5], F. Chevallier[6], J. Notholt[7], N. Deutscher[7,11], T. Warneke[7], F. Hase[8], R. Sussmann[8], S. Kawakami[9], R. Kivi[10], D. W. T. Griffith[11], and V. Velazco[11]

[1]Earth Observation Science, Department of Physics and Astronomy, University of Leicester, Leicester, UK
[2]National Centre for Earth Observation, Department of Physics and Astronomy, University of Leicester, Leicester, UK
[3]School of GeoSciences, University of Edinburgh, Edinburgh, UK
[4]National Centre for Earth Observation, School of GeoSciences, University of Edinburgh, Edinburgh, UK
[5]European Commission Joint Research Centre, Institute for Environment and Sustainability, Ispra, Italy
[6]Lab. des Sciences du Climat et de l'Environnement, CNRS, Gif-sur-Yvette, France
[7]Institute of Environmental Physics, University of Bremen, Bremen, Germany
[8]Karlsruhe Institut für Technologie, Karlsruhe, Germany
[9]Japan Aerospace Exploration Agency (JAXA), Tsukuba, Japan
[10]Finnish Meteorological Institute, Arctic Research, Sodankylä, Finland
[11]School of Chemistry, University of Wollongong, Wollongong, Australia

Correspondence to: R. J. Parker (rjp23@le.ac.uk)

Received: 5 May 2015 – Published in Atmos. Meas. Tech. Discuss.: 17 June 2015
Revised: 20 October 2015 – Accepted: 29 October 2015 – Published: 17 November 2015

Abstract. We present 5 years of GOSAT XCH_4 retrieved using the "proxy" approach. The Proxy XCH_4 data are validated against ground-based TCCON observations and are found to be of high quality with a small bias of 4.8 ppb (∼ 0.27 %) and a single-sounding precision of 13.4 ppb (∼ 0.74 %). The station-to-station bias (a measure of the relative accuracy) is found to be 4.2 ppb. For the first time the XCH_4 / XCO_2 ratio component of the Proxy retrieval is validated (bias of 0.014 ppb ppm^{-1} (∼ 0.30 %), single-sounding precision of 0.033 ppb ppm^{-1} (∼ 0.72 %)).

The uncertainty relating to the model XCO_2 component of the Proxy XCH_4 is assessed through the use of an ensemble of XCO_2 models. While each individual XCO_2 model is found to agree well with the TCCON validation data ($r = 0.94$–0.97), it is not possible to select one model as the best from our comparisons. The median XCO_2 value of the ensemble has a smaller scatter against TCCON (a standard deviation of 0.92 ppm) than any of the individual models whilst maintaining a small bias (0.15 ppm). This model median XCO_2 is used to calculate the Proxy XCH_4 with the maximum deviation of the ensemble from the median used as an estimate of the uncertainty.

We compare this uncertainty to the a posteriori retrieval error (which is assumed to reduce with sqrt(N)) and find typically that the model XCO_2 uncertainty becomes significant during summer months when the a posteriori error is at its lowest due to the increase in signal related to increased summertime reflected sunlight.

We assess the significance of these model and retrieval uncertainties on flux inversion by comparing the GOSAT XCH_4 against modelled XCH_4 from TM5-4DVAR constrained by NOAA surface observations (MACC reanalysis scenario S1-NOAA). We find that for the majority of regions the differences are much larger than the estimated uncertainties. Our findings show that useful information will be provided to the inversions for the majority of regions in addition to that already provided by the assimilated surface measurements.

Published by Copernicus Publications on behalf of the European Geosciences Union.

1 Introduction

Atmospheric methane (CH_4) contributes significantly to the Earth's radiative forcing budget (Myhre et al., 2013), making it the second most important anthropogenic greenhouse gas after carbon dioxide (CO_2). The major sources of atmospheric methane include wetland emission, rice production, enteric fermentation (cattle), termites, biomass burning, fossil fuel production, and waste (Bousquet et al., 2006). There remains, however, a large degree of uncertainty on the magnitude of these individual sources (Kirschke et al., 2013).

The lifetime of CH_4 in the atmosphere is mainly controlled by its reaction with the hydroxyl free radical (OH), resulting in an atmospheric lifetime of approximately 9 years (Prather et al., 2012). Given its long atmospheric lifetime, there is a need for long-term global measurements to fully understand how the atmospheric distribution of CH_4 is evolving with time. Indeed, recent unexpected variability in the atmospheric growth rate of methane has emphasised gaps in our current understanding (Rigby et al., 2008; Dlugokencky et al., 2009; Nisbet et al., 2014).

In order to begin to understand the spatio-temporal distribution of atmospheric methane, regular global satellite observations of CH_4 can be coupled with highly precise but geographically sparse surface concentration data. Through the combination of both data sources, the large uncertainties related to the upscaling of surface concentration data can be minimised whilst also obtaining information in remote regions where surface measurements are not available.

Various studies have demonstrated the utility of such space-borne measurements in determining the regional surface fluxes of methane using data from the SCIAMACHY (Bergamaschi et al., 2007, 2009, 2013; Houweling et al., 2014) and Greenhouse gases Observing SATellite (GOSAT) (Fraser et al., 2013; Cressot et al., 2014; Monteil et al., 2013; Alexe et al., 2015) instruments.

The SCIAMACHY instrument operated onboard ENVISAT and provided a 9-year record (2003–2012) of global methane total column observations (Schneising et al., 2011; Frankenberg et al., 2011). The continuation of this time series of space-based observations was ensured by the launch of the first dedicated greenhouse gas measuring satellite, the Japanese GOSAT, in 2009 (Yokota et al., 2009). GOSAT provides global coverage with a 3-day repeat cycle and was designed with the intention of characterising continental-scale sources and sinks.

In a previous work (Parker et al., 2011) we presented the first year of our global short-wave infrared (SWIR) measurements of the dry-air column-averaged mole fraction of CH_4 (XCH_4) from the GOSAT mission using the "proxy" retrieval approach. This data product has subsequently been developed (Buchwitz et al., 2013) and validated (Dils et al., 2014) as part of the ESA Climate Change Initiative Greenhouse Gas project and we now report an assessment of the full 5-year data set for version 5.0 of the University of Leicester GOSAT Proxy XCH_4 data product.

This work is motivated by the desire to better understand the uncertainty characteristics of the Proxy XCH_4 data for use within flux inversion systems, especially relating to uncertainties introduced by the model XCO_2.

In Sect. 2 we describe the retrieval approach, including details of the updates since the original version of the University of Leicester GOSAT Proxy XCH_4 data (Parker et al., 2011). In Sect. 3 we compare both the Proxy XCH_4 and the XCH_4/XCO_2 ratio against the ground-based validation data. In Sect. 4 we assess the CO_2 model component of the Proxy XCH_4 for the first time, with Sect. 5 then discussing the associated uncertainty of the final Proxy XCH_4 product and its utility in constraining surface fluxes within an inversion framework. Finally, we conclude the paper in Sect. 6 and provide recommendations for data users.

2 University of Leicester GOSAT Proxy XCH_4 retrieval updates

The University of Leicester GOSAT Proxy XCH_4 retrieval utilises the Orbiting Carbon Observatory (OCO) "full physics" retrieval algorithm, developed for the original NASA OCO mission to retrieve XCO_2 (dry-air column-averaged mole fraction of CO_2) from a simultaneous fit of SWIR O_2 and CO_2 bands and has subsequently been modified to operate on GOSAT spectral data.

Full details of the OCO retrieval algorithm can be found in O'Dell et al. (2012). In short, the retrieval algorithm utilises an iterative retrieval scheme based on Bayesian optimal estimation to estimate a set of atmospheric, surface, and instrument parameters from the measured spectral radiances, referred to as the state vector. The state vector of our retrieval consists of 20-level profiles for CH_4 and CO_2 volume mixing ratios (vmr), profile scaling factors for H_2O vmr, and temperature, surface albedo, and spectral dispersion.

Rather than perform the "full physics" retrieval as typically used for CO_2 (Connor et al., 2008; Boesch et al., 2011), an alternative approach is possible for CH_4, the so-called "proxy" method. First used for the retrieval of XCH_4 from SCIAMACHY (Frankenberg et al., 2006), this approach uses the fact that there exists CO_2 and CH_4 spectral signatures located close together at around 1.6 µm and hence the majority of atmospheric scattering and instrument effects will be similar between the two bands. The ratio of the retrieved XCH_4 / XCO_2 should cancel modifications to the length of the light path that are experienced due to scattering (Butz et al., 2010), with the CO_2 effectively acting as a "proxy" for the unknown light-path enhancements. As CO_2 is known to vary much less than CH_4, the final XCH_4 product can be obtained by multiplying this XCH_4 / XCO_2 ratio by a model CO_2 value, typically taken from a global chemistry transport model (Eq. 1).

$$\text{Proxy}_{\text{XCH}_4} = \frac{[\text{XCH}_4]}{[\text{XCO}_2]} \times \text{Model}_{\text{XCO}_2} \quad (1)$$

The "proxy" retrieval approach has various advantages over the full physics approach (Schepers et al., 2012). Because there is no reliance on an explicit a priori knowledge of the aerosol distribution, the proxy approach is more robust in the presence of aerosols and also far less sensitive to instrumental issues or inconsistent radiometric calibration between the spectral bands than is the case for the full physics approach. Additionally, as moderate scattering from aerosols will be cancelled out and still result in an accurate retrieval of XCH_4, the number of successful soundings for the proxy approach is typically much higher than for the full physics approach which requires far stricter post-filtering. This leads not only to more soundings in general but also to more soundings over regions where very little full physics data may be available, such as in the tropics.

The main disadvantage with the proxy approach is that it is reliant on an accurate, unbiased model XCO_2 data set to convert the XCH_4 / XCO_2 ratio back into an XCH_4 quantity; otherwise errors relating to the model XCO_2 may be folded into the final XCH_4 result. Here we present assessments of the different uncertainties to determine the importance of this aspect of the Proxy XCH_4 data.

We process the latest versions of the GOSAT Level 1B files (version 161.160) acquired directly from the NIES Large Volume Data Server and apply the recommended radiometric calibration and radiometric degradation correction as per Kuze et al. (2014).

For the spectroscopic inputs we use v4.2.0 of the OCO line lists with CH_4 taken from the Total Carbon Column Observing Network (TCCON) line lists (version "20120409"). The a priori pressure, temperature, and water vapour is taken from the ECMWF ERA-Interim data (Dee et al., 2011). For the CO_2 a priori we use the MACC-II CO_2 inversion (v13r1) and for the CH_4 we use the MACC-II CH_4 inversion (v10-S1NOAA, using 2012 data for 2013) but here we adjust the stratospheric methane using a specialised full chemistry run (run ID 563) of the TOMCAT stratospheric chemistry model from the University of Leeds (Chipperfield, 1999). This TOMCAT model run has been validated against ACE-FTS observations and was found to provide a more accurate representation of the stratosphere.

The spectral noise is estimated from the standard deviation of the out-of-band signal. Spectra over ocean or with a signal-to-noise ratio (SNR) below 50 are removed. Cloud-contaminated scenes are removed by the comparison of a clear-sky surface pressure retrieval from the O_2 A-band to the ECMWF surface pressure for the relevant measurement time and location. A scene is determined to be cloudy when the retrieved surface pressure differs by more than 30 hPa from the estimated ECMWF surface pressure. This relatively loose threshold is allowed as the proxy retrieval approach remains relatively robust in the presence of near-surface clouds. The average difference between our retrieved surface pressure and ECMWF after filtering for cloud is approximately 3 hPa with a standard deviation of below 10 hPa, with the offset from 0 hPa being attributed to spectroscopic uncertainties in the O_2 cross-sections. The Proxy XCH_4 retrieval is performed for all scenes that are deemed to be sufficiently cloud free.

After filtering for signal-to-noise, cloud, and data quality we are left with 1 032 760 XCH_4 retrievals over land between April 2009 and December 2013. Figure 1 shows global maps of the Proxy XCH_4 for each season and compares it to the MACC-II model XCH_4 data. Both model and observation show the XCH_4 variability in time and space, in particular with the large emissions of methane from wetland and rice cultivation over India and S.E. Asia.

3 Validation of the Proxy XCH_4 and XCH_4/XCO_2 ratio

This section presents the validation of the University of Leicester GOSAT Proxy XCH_4 v5.0 data through comparison to observations from the ground-based TCCON. In addition, for the first time the XCH_4 / XCO_2 ratio itself, the core component of the Proxy XCH_4 data, is validated against the corresponding TCCON data.

TCCON is a global network of ground-based high-resolution Fourier transform spectrometers recording direct solar spectra in the near-infrared spectral region (Wunch et al., 2011a). The TCCON data are calibrated to World Meteorological Organization (WMO) standards by calibration against aircraft measurements (Wunch et al., 2010). Although it should be noted that this aircraft calibration does not measure the whole column, the TCCON data are the standard against which current satellite observations of greenhouse gases are validated (Cogan et al., 2012; Wunch et al., 2011b; Dils et al., 2014).

To date, all previous validation of satellite greenhouse gas observations against TCCON has used TCCON data that were affected by instrumental biases relating to a laser sampling error which resulted in an XCO_2 error of approximately 0.26 % (1 ppm) (Messerschmidt et al., 2010). Although the corresponding XCH_4 error was not quantified, it is expected that it would be of similar magnitude (i.e. 1 part in 400). The latest, recently released, version of the TCCON data (GGG2014) incorporates a correction for the laser sampling errors and any remaining bias is expected to be small.

Figure 2 shows the GGG2014 TCCON XCH_4 data and the Proxy XCH_4 plotted as time series for each TCCON site. The mean GOSAT−TCCON difference, the standard deviation of the GOSAT−TCCON difference, the correlation coefficient, and the number of soundings are all provided for each site.

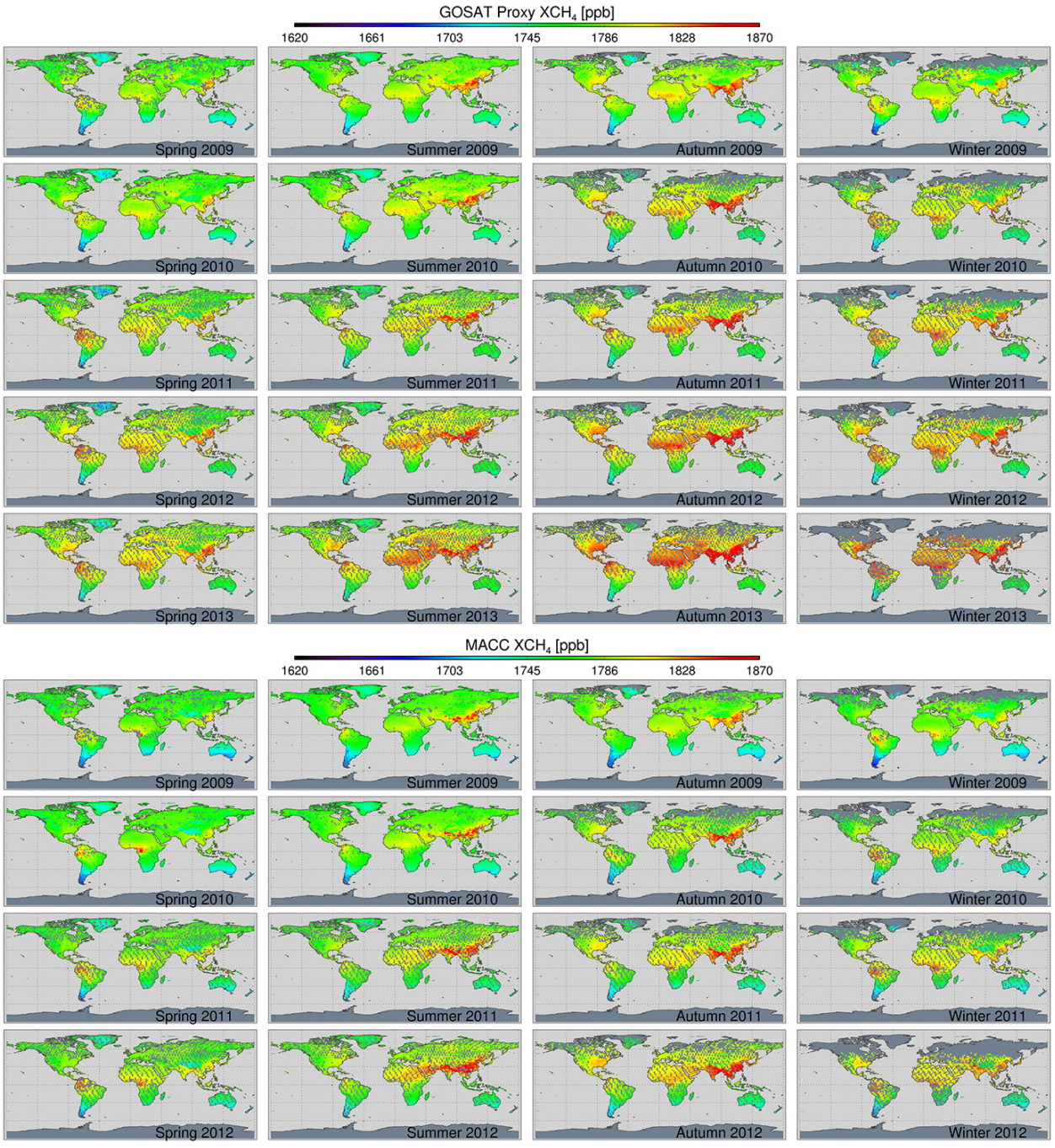

Figure 1. Seasonal global maps of the University of Leicester GOSAT Proxy XCH_4 (top) and the MACC-II (bottom) model XCH_4 data (v10-S1NOAA). Both model and observation show the XCH_4 variability in time and space, in particular with the large emissions of methane from wetland and rice cultivation over India and S.E. Asia. Note that GOSAT changed their pointing pattern in August 2010 from five across-track points to three across-track points, resulting in a change in spatial coverage.

Figure 3 (top) shows the correlation between the GGG2014 TCCON XCH_4 data and the Proxy XCH_4 values within $\pm 5°$ of each TCCON site and a temporal coincidence of ± 2 h. It should also be noted that for all TCCON comparisons, the difference inherent in the data due to using different a priori has been compensated for (as discussed in Rodgers (2000), by replacing the a priori used in the GOSAT retrievals with the TCCON a priori after the retrieval has been performed) which typically increases the GOSAT XCH_4 data by an average of between 0 and 5 ppb with the larger effect seen at more northernly TCCON stations. We use all TCCON sites where version GGG2014 has been processed at the time

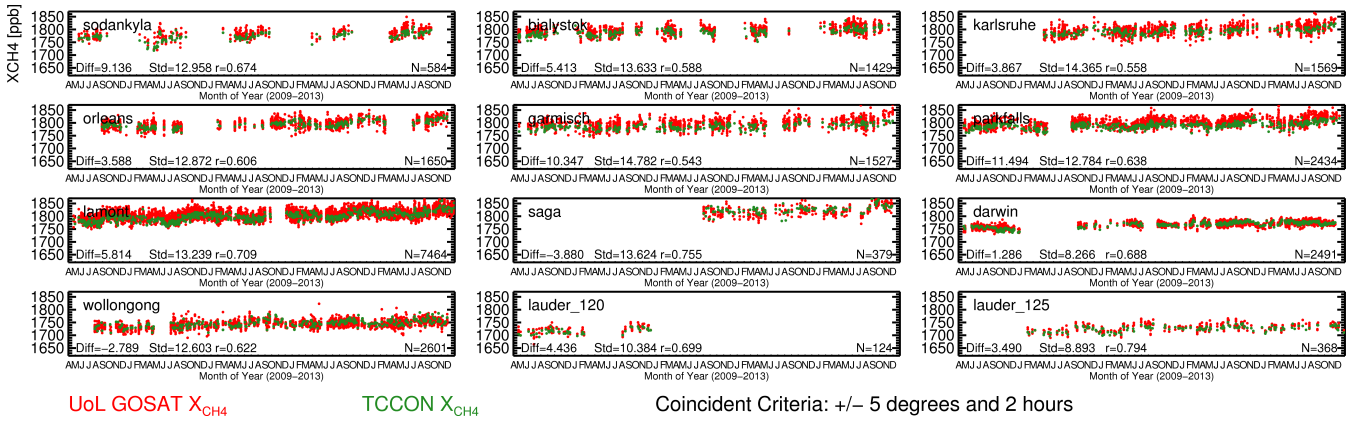

Figure 2. GGG2014 TCCON XCH_4 data and the Proxy XCH_4 plotted as time series for each TCCON site. The mean GOSAT−TCCON difference, the standard deviation of the GOSAT−TCCON difference, the correlation coefficient, and the number of soundings are all provided for each site.

of writing that contain data during the GOSAT time period (2009–2014). This results in 11 TCCON stations ranging from Sodankylä, Finland, at 67.4° N to Lauder, New Zealand, at 45.0° S. The correlation between the GOSAT and TCCON data is reasonable/good across all sites, ranging from 0.54 at Karlsruhe to 0.79 at Lauder with an overall correlation coefficient of 0.87 between 22 619 points. The overall bias is found to be 4.8 ppb with an overall single measurement precision of 13.4 ppb (ranging from 8.3 ppb at Darwin to 14.9 ppb at Garmisch). The station-to-station bias, which is an indication of the relative accuracy, is calculated as the standard deviation of the individual site biases and is found to be just 4.2 ppb.

In addition to the validation of the Proxy XCH_4 data, we also present for the first time the validation of the XCH_4 / XCO_2 ratio. This ratio is the quantity directly retrieved from the satellite measurement, is independent of any model XCO_2, and has recently itself been used directly within a flux inversion study (Fraser et al., 2014). The correlation coefficient across all stations is found to be 0.88 (ranging from 0.6 at Wollongong to 0.88 at Sodankylä) with a mean bias of 0.014 ppb ppm^{-1} and a single-sounding precision of 0.033 ppb ppm^{-1} (ranging from 0.20 ppb ppm^{-1} at Darwin to 0.037 ppb ppm^{-1} at Garmisch). The statistics for the XCH_4 / XCO_2 ratio are therefore comparable to those of the Proxy XCH_4 itself, suggesting that the majority of the variation is from the satellite retrieval itself and not introduced by the model XCO_2. The next section investigates this aspect in more detail.

4 Assessing the CO_2 model ensemble component

In Sect. 3 the final Proxy XCH_4 and the XCH_4 / XCO_2 component were both validated against the TCCON data. In this section we validate the remaining component of the proxy product from Eq. (1), namely the model XCO_2.

As discussed in Sect. 2, this update to the University of Leicester GOSAT Proxy XCH_4 data uses an ensemble of model XCO_2 data to act as the model XCO_2 component. We utilise the XCO_2 from three state-of-the-art global transport models which all assimilate surface in situ measurements; GEOS-Chem (University of Edinburgh – Feng et al., 2011, v1.50), MACC-II (Chevallier et al., 2010, v14r1) and CarbonTracker (NOAA – Peters et al., 2007, vCT2013B). These model runs have assimilated similar surface measurements but not necessarily from all of the same data sets or the same locations. The models also have different spatial resolutions and different temporal coverage (GEOS-Chem: 2009–2011, 5° × 4°; CarbonTracker: 2009–2012, 3° × 2°; MACC-II: 2009–2012, 3.75° × 1.89°). Where the model does not cover the full GOSAT time period studied here, the data from the previous year are used and adjusted by the NOAA annual growth rate.

The main concern with using modelled XCO_2 data for the proxy method is that the additional uncertainty added to the final proxy data product is difficult to determine. Where the model XCO_2 data are constrained by surface data there can be a high degree of confidence that the model data are close to representing the true value of CO_2; however, it is away from such regions where there is a possibility of adding additional biases into the Proxy XCH_4 data. The TCCON stations are mostly in regions that are also well constrained by surface in situ measurements and hence the model CO_2 data should be well constrained, at least at the surface level, and it is therefore expected to reasonably reproduce the TCCON column data. Figure 4 confirms that this is the case. As the model XCO_2 is used as a component in the proxy retrievals, the models are treated as "pseudo-measurements" and validated in the same way as the satellite data in order to maintain consistency with the satellite validation. The model XCO_2 data sampled at each GOSAT measurement point within ± 2° of each TCCON station are found to agree well with the

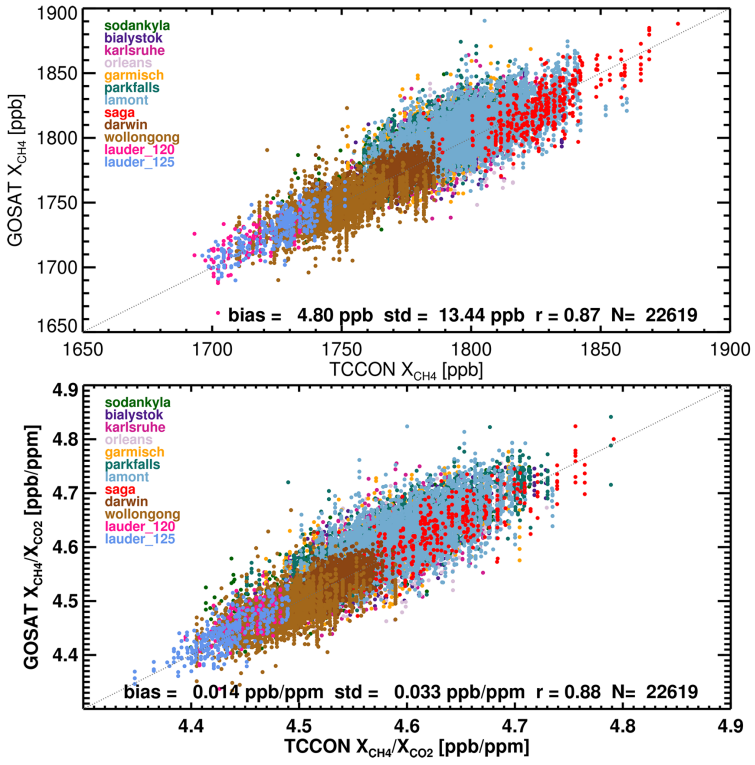

Figure 3. Correlation plot of the Proxy XCH_4 (top) and the XCH_4/XCO_2 ratio (bottom) data against TCCON ground-based FTS data at 11 TCCON sites. The overall bias, standard deviation (single-sounding precision), correlation coefficient, and total number of soundings are provided. Note that the Lauder TCCON station upgraded the instrument from a Bruker 120 to a Bruker 125 in February 2010 and these two data sets are displayed separately.

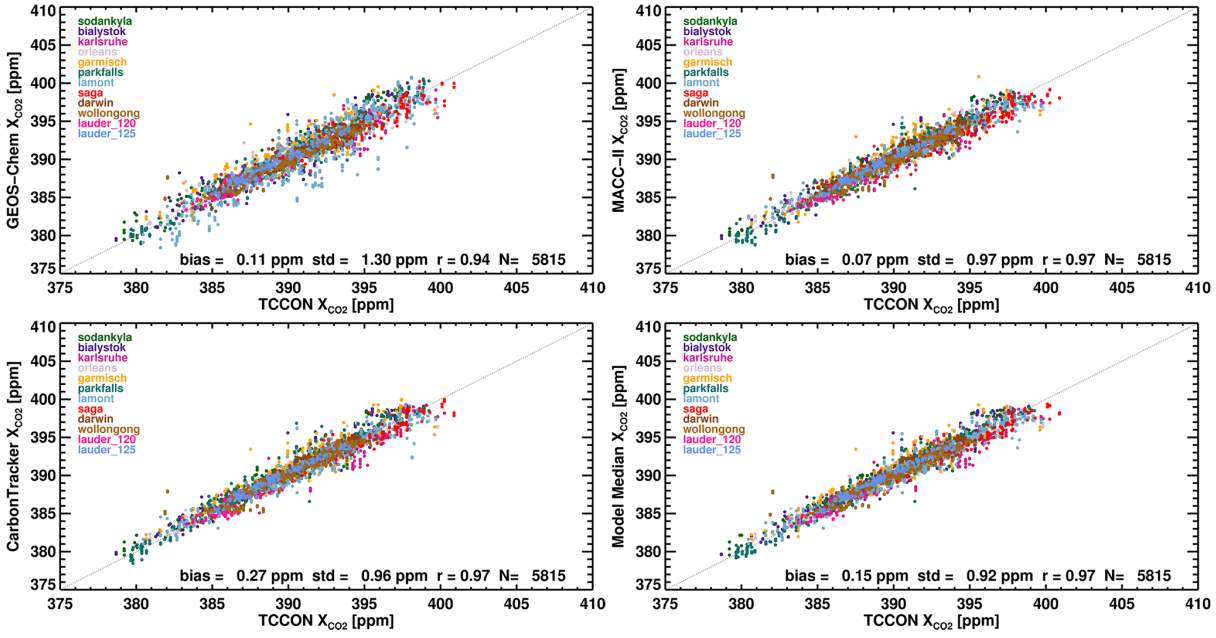

Figure 4. Correlation plot of the model XCO_2 data for GEOS-Chem, MACC-II, CarbonTracker, and the ensemble median against TCCON ground-based FTS data at 11 TCCON sites. The overall bias, standard deviation (single-measurement precision), correlation coefficient, and total number of soundings are provided separately.

TCCON data, with the correlation coefficients ranging from 0.94 (GEOS-Chem) to 0.97 (MACC-II and CarbonTracker). Similarly the precision and bias to TCCON are both found to be small (ranging from 0.97 to 1.3 and 0.07 to 0.27 ppm respectively). The relative accuracies (the standard deviation of the individual site biases) are similar at around 0.5 ppm, with CarbonTracker and GEOS-Chem performing slightly better than MACC-II. Another metric to assess the models is how often they provide the median value of the ensemble. CarbonTracker (41 %) and MACC-II (36 %) tend to provide the median value more often than GEOS-Chem (22 %) but this can vary per site with the contribution from MACC-II as low as 27 % at Darwin (and CarbonTracker at 60 %) and conversely as high as 44 % at Wollongong (with CarbonTracker only 21 %). This provides further indication that no one model can be determined to be the "best".

For a more detailed analysis of the performance of the different XCO_2 models please see Table A1 in Appendix A. In short, none of the models are found to consistently be superior over the other models. GEOS-Chem typically has the highest scatter against TCCON but also has the smallest bias at 5 out of 12 of the sites. MACC-II has the smallest bias at seven sites but the highest bias at four of the sites. CarbonTracker has the highest bias at seven of the sites but also has the smallest scatter at eight of the sites. Whilst the absolute bias in the calculated median XCO_2 is typically not quite as small as the best of the individual models, the scatter in the median is better than (or the same as) the best scatter from any of the individual models at every site except Lauder_120 (where the time series is the shortest) and even there it is only worse than the best model by less than 0.1 ppm.

The above has demonstrated that it is not a simple decision to determine which model most accurately represents the true atmosphere, even in locations where all of the models have been constrained by (often the same) surface measurements and high-quality validation data are available. In more remote regions where we neither have validation data nor surface measurements to constrain the models, this inconsistency between the models becomes more pronounced. It is this uncertainty in model XCO_2 in regions away from the available validation data that we attempt to address through the use of the XCO_2 model ensemble. Each of the three XCO_2 models are sampled at every GOSAT time and location and convolved with the scene-specific GOSAT averaging kernels. The median value of the three model values is used as the model XCO_2 in calculating the final Proxy XCH_4. However, we also define the uncertainty on this median XCO_2 as the maximum of the absolute differences of each individual model to the median value.

We have already demonstrated that the models all well reproduce the validation data at TCCON sites without any one model identified as being better than the others from our comparisons. Where the models all agree well with each other away from the validation sites, the assumption is that the models are accurately representing the true atmosphere. Where the models disagree with each other, we do not know which model is correct in the absence of further validation data and in some cases the discrepancy between models can be very large (i.e. > 4 ppm). In such cases where no validation is possible, the best estimate of the uncertainty in the model XCO_2 data is obtained by examining the difference of the model data around the median value. Figure 5 shows global maps of this estimated model uncertainty for each season. There are clear spatial/temporal patterns in the distribution of this model uncertainty. During March–May (boreal "spring"), there is a large uncertainty (> 2 ppm) over India and the African regions typically associated with biomass burning. There is also a moderate level of uncertainty (> 1 ppm) over Europe, South America, and for the latter years over North America and Australia. For the summer months (June–August) it is the Eurasian region, extending from the Ural mountains eastwards through Siberia and northern China, where the model uncertainty is largest at over 2 ppm. This is to be expected as in the Northern Hemisphere it is the period of greatest photosynthetic activity and the model sensitivity to the underlying mechanisms is likely to be largest. During boreal autumn (September–November), the uncertainty in the Northern Hemisphere is vastly reduced again, with India being the major region of uncertainty along with South America and regions of biomass burning in Africa. Winter is similar to autumn, with all three models in very good agreement with each other in the Northern Hemisphere, with only S.E. Asia showing a moderate level of uncertainty. In the Southern Hemisphere, again South America and southern Africa show moderate uncertainty which appears to be linked to emissions from biomass burning.

This section has shown that the estimated uncertainty of the model XCO_2 can vary greatly in time and space. When considering the implication of this uncertainty on flux inversions of the Proxy XCH_4 data, the relative importance of the different uncertainties must be considered. The following section investigates the distribution of the model XCO_2 uncertainty and judges its relative importance against the a posteriori error from the retrieval itself. Finally, both of these uncertainties are assessed against the difference to modelled XCH_4 already constrained by surface observations to determine the utility of the satellite data despite the presence of these uncertainties.

5 Assessing the relative uncertainties

In order to assess the importance of the uncertainty of the model XCO_2, we bin the three model fields into $4^\circ \times 5^\circ$ grid boxes over 8-day time steps and calculate the maximum difference of the three-model ensemble from the median value to use as an estimate of the uncertainty in the model values. We convert this uncertainty in model XCO_2 into an uncertainty in XCH_4 by multiplying each point by its respective retrieved XCH_4 / XCO_2 amount. We also calculate the av-

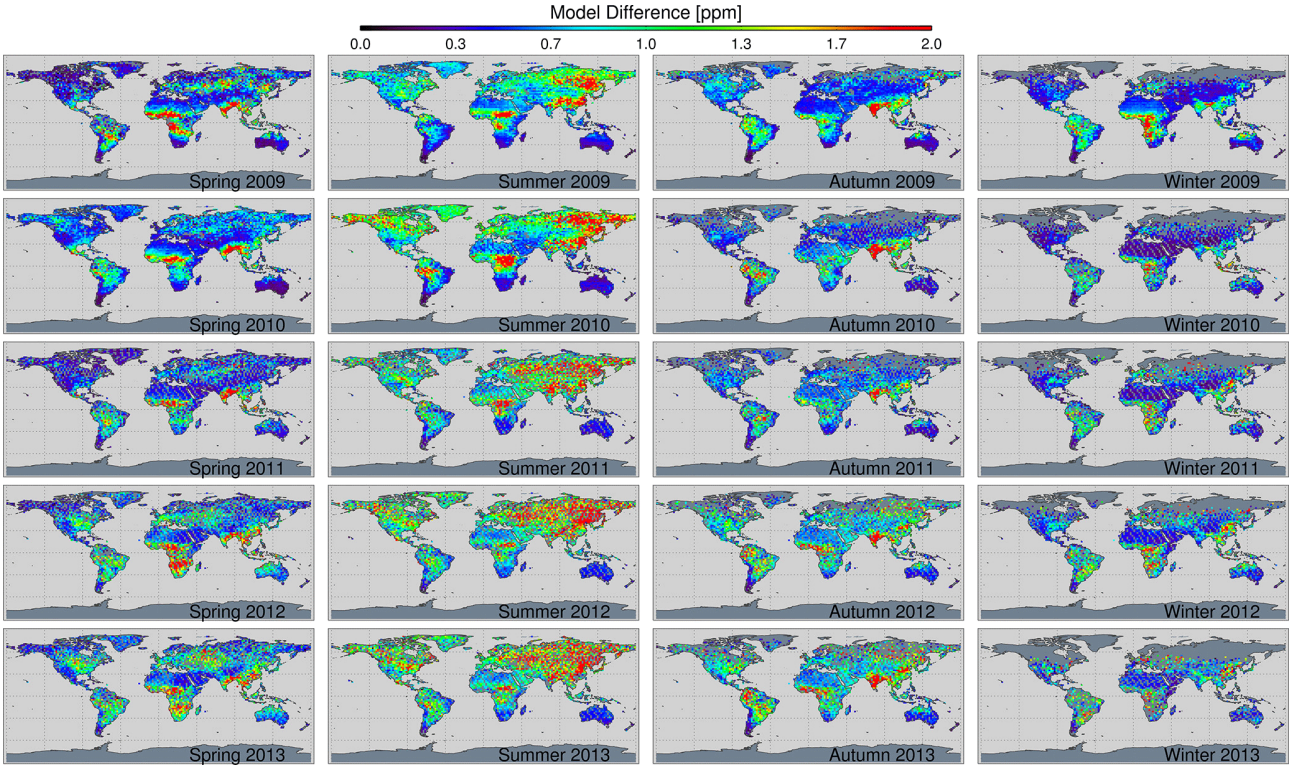

Figure 5. Seasonal maps of the model difference, defined as the maximum absolute difference of the three-model ensemble from the median. All individual soundings have been averaged into $2^\circ \times 2^\circ$ grid boxes over each season. The largest uncertainties occur in regions where the CO_2 variability is expected to be highest and the models are unconstrained by surface measurements.

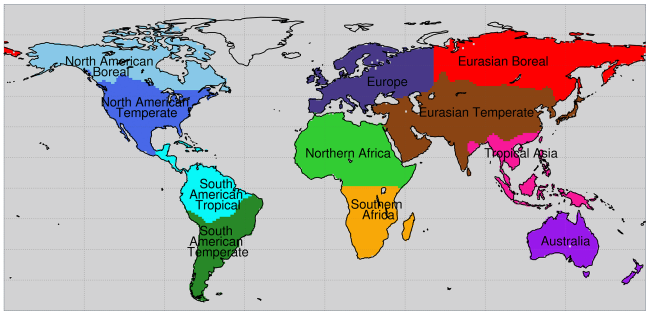

Figure 6. The Transcom regions over which the $4^\circ \times 5^\circ$ gridded data are then averaged in Fig. 7.

erage a posteriori error for the same data. Unlike the more systematic XCO_2 model uncertainty, the a posteriori error should be close to random and hence reduce approximately with the square root of the number of soundings being averaged. If the error does not reduce as much, the model XCO_2 component would then contribute even less to the total, leading to this assumption being a "worst case" scenario for the effect of the model XCO_2 uncertainty. These $4^\circ \times 5^\circ$ grid boxes are then themselves averaged over the Transcom regions (Gurney et al., 2002) as defined in Fig. 6.

In Fig. 7, the red line shows the mean of the Proxy XCH_4 random (a posteriori) error from each $4^\circ \times 5^\circ$ box averaged over each Transcom region with the green line representing the estimated uncertainty related to the model XCO_2. The majority of regions exhibit a similar trend over time. The a posteriori error peaks in the winter months when the SNR of the measurement is at its lowest and is at a minimum during the summer months when the SNR is at a maximum. This seasonal effect is more pronounced at higher latitudes which experience a greater degree of variability of sunlight throughout the year. Conversely, the XCO_2 model uncertainty follows biospheric activity with the uncertainty largest during the summer months when the XCO_2 variability is at a maximum and reduces to a minimum in the winter months when biospheric activity is lower. This leads to the situation where the a posteriori error dominates the model uncertainty in winter months but during summer months the model uncertainty can be comparable to, or even exceed, the a posteriori error. Taking the North America Temperate region as an example, during winter the a posteriori error can reach up to 8 ppb with the error from the model XCO_2 significantly lower with values less than 2 ppb. In contrast, during the summer months, the a posteriori error reduces to around 5 ppb but the error for the model XCO_2 increases to 5 ppb, meaning that both become significant components of the overall uncertainty.

We have shown that the uncertainty related to the XCO_2 model can, particularly in the Northern Hemisphere during summer months, be of comparable magnitude to the a posteriori retrieval error. However, that in itself does not preclude the data from adding useful information to a CH_4 flux inversion.

The MACC-II model XCH_4 (v10-S1NOAA) data have assimilated NOAA surface measurements at background sites and hence are well constrained in the remote atmosphere (Bergamaschi et al., 2013). Here we calculate the difference between the MACC XCH_4 model field and the GOSAT Proxy XCH_4 data for each GOSAT measurement (referred to from here as ΔXCH_4). We then aggregate these differences in the same way as the model XCO_2 uncertainties. Note that the MACC XCH_4 model data are currently only available until the end of 2012. As some inversion systems will perform a simple (e.g. latitudinal) bias correction, the calculated retrieval a posteriori and model XCO_2 uncertainties can potentially be much lower than the ΔXCH_4 value but still not provide information to the inversion. For this reason, it is also important to consider both the mean ($\mu_{\Delta XCH_4}$) and the standard deviation ($\sigma_{\Delta XCH_4}$) of the ΔXCH_4. To determine whether the GOSAT data are capable of providing information to the inversion, we compare the a posteriori and model XCO_2 uncertainties to the $\mu_{\Delta XCH_4}$ and $\sigma_{\Delta}XCH_4$ values as shown in Fig. 7, with the seasonal averages for all of these values presented in Table A2.

It should be noted here that the absolute values are not necessarily quantitatively comparable when taking into account how an inversion system will use the two different quantities. The a posteriori error of the retrieved XCH_4 is an indication of the weighting that the inversion will give to an observation over the a priori, with a smaller value indicating that the inversion will "trust" the observation more. The ΔXCH_4 is an indication of how much the inversion needs to adjust the fluxes in order to match the observation. However, if the estimated uncertainties are significantly less than the $\mu_{\Delta XCH_4}$ and $\sigma_{\Delta XCH_4}$ values it is expected that the observations should provide value to the inversion. It should also be noted that this bias term ($\mu_{\Delta XCH_4}$) may also reflect systematic biases in the XCH_4 model due to, for example, errors in the vertical model profile whilst the sigma term ($\sigma_{\Delta XCH_4}$) may also relate to subgrid-scale variations which are unresolved at the model resolution.

For the North American Boreal region, both the $\mu_{\Delta XCH_4}$ and $\sigma_{\Delta XCH_4}$ values are very similar in terms of phase and magnitude to the a posteriori uncertainty with the $\sigma_{\Delta XCH_4}$ ranging from an average of 9.6 ppb in summer to 14.5 ppb in winter compared to the a posteriori uncertainty that ranges from 6.6 ppb in summer to 10.8 ppb in winter. This suggests that regardless of the contribution to the uncertainty from the XCO_2 model, it would be difficult for the satellite data to inform the inversion any further than the in situ data already do. However, this is not the case for the North American Temperate region where the $\mu_{\Delta XCH_4}$ (7.4–11.6 ppb) and $\sigma_{\Delta XCH_4}$ (8.4–10.0 ppb) are far larger than the total uncertainty (6.0–6.9 ppb) for much of the year. Both South American regions exhibit more complicated behaviour with far less of an apparent seasonality in the $\mu_{\Delta XCH_4}$. Instead, for most years $\mu_{\Delta XCH_4}$ is much higher than the uncertainties (which themselves do not exhibit much seasonality in these regions). However, the year 2010 seems to be an anomalous year where the $\mu_{\Delta XCH_4}$ data are much more in agreement and in this year the difference is of comparable magnitude to the uncertainties with values between 4 and 8 ppb. The $\sigma_{\Delta XCH_4}$ does exhibit more seasonality than the $\mu_{\Delta XCH_4}$ and is again considerably higher than the estimated uncertainties (7–20 ppb vs. 5–6 ppb). In combination, this suggests that the GOSAT observations over South America should add considerable information to the inversion.

For Northern Africa, both the a posteriori error and the uncertainty related to the XCO_2 model are small due to the high SNR over the Sahara and the low CO_2 variability respectively (with seasonal average values ranging from 3.3 to 3.6 ppb for the a posteriori error and from 2.8 to 4.6 ppb for the model XCO_2 error). In contrast, the $\mu_{\Delta XCH_4}$ (7.2–12.3 ppb) and $\sigma_{\Delta XCH_4}$ (4.9–8.4 ppb) values over this region are relatively large with a high degree of temporal variability, suggesting that the satellite data should add considerable value in constraining the inversion over this region. One complication is that GOSAT operates in a "medium gain" mode over the desert and hence may exhibit different instrumental biases over such regions but, due to the proxy method, any such differences in instrumental biases that relate to light-path modification should be minimised. Southern Africa shows similar behaviour with the total uncertainty being low (seasonal averages of 5.1–7.3 ppb) compared to the much larger $\mu_{\Delta XCH_4}$ (12.6–19.8 ppb) and $\sigma_{\Delta XCH_4}$ (5.7–10.7 ppb) values, again indicating that considerable value is present in the satellite data.

The Eurasian Boreal region behaves similarly to the North American Boreal region. The $\mu_{\Delta XCH_4}$ and $\sigma_{\Delta XCH_4}$ is of similar phase and magnitude to the retrieval a posteriori error, suggesting little information will be added to any inversion over this region beyond what is available from the in situ measurements. In contrast, the $\mu_{\Delta XCH_4}$ values over the Eurasian Temperate region show a large variability with the differences in winter months much larger than the total uncertainty (9.9 ppb vs. 5.8 ppb), while in summer months the magnitudes become much more similar (5.5 ppb vs. 7.3 ppb). Interestingly, the $\sigma_{\Delta XCH_4}$ values appear to be of similar magnitude (5–20 ppb) but directly out of phase with the $\mu_{\Delta XCH_4}$ values. Even during summer months when the a posteriori (4.3 ppb) and model XCO_2 (5.8 ppb) uncertainties are comparable to the $\mu_{\Delta XCH_4}$ (5.5 ppb), the high variability in the ΔXCH_4 values, as indicated by $\sigma_{\Delta XCH_4}$ values of up to 20 ppb (and a summertime mean value of 15.0 ppb), suggests that the observations are capable of providing useful information to the inversion.

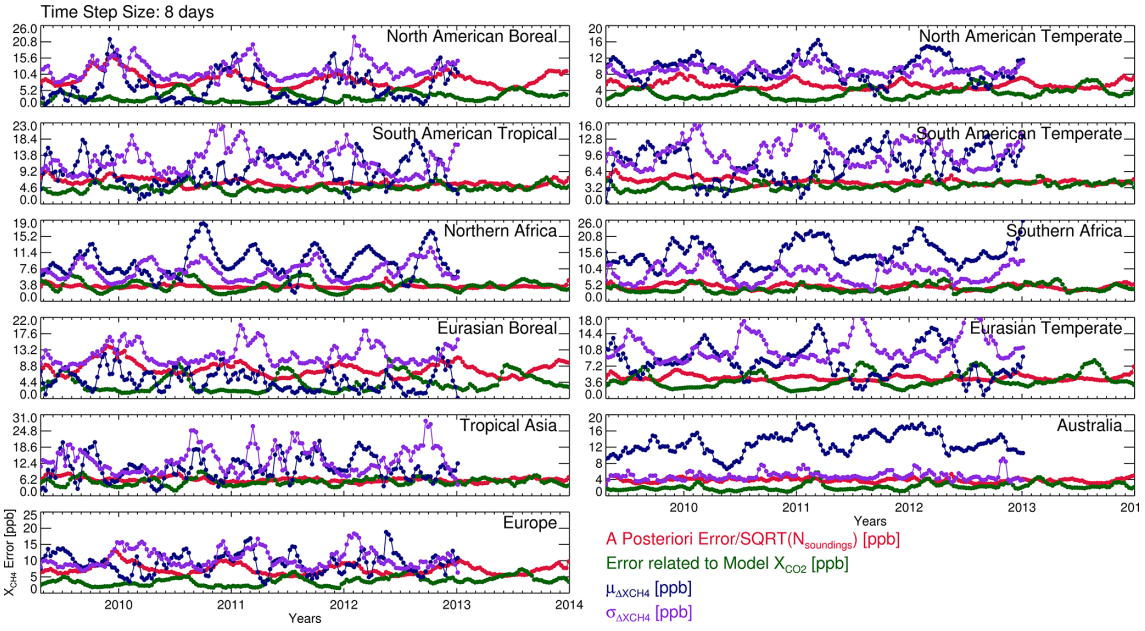

Figure 7. Time series for each Transcom region showing the a posteriori retrieval error (red), the estimated uncertainty from the model XCO_2 (green), and the mean (navy) and standard deviation (purple) of the difference between the GOSAT and MACC-II XCH_4. The a posteriori error is assumed to be a random error and hence reduces with the square root of the number of measurements whilst the XCO_2 model uncertainty is expected to be a systematic error and hence does not reduce.

The Tropical Asian region, which encompasses parts of India, China, and Indonesia, typically has low values for both the a posteriori (5.6–6.9 ppb) and XCO_2 model (4.4–6.0 ppb) uncertainties, with neither exhibiting much seasonal variability. The $\mu_{\Delta XCH_4}$ and $\sigma_{\Delta XCH_4}$ values however are much more variable (8.9–11.7 and 9.0–16.8 ppb) and generally much higher than the uncertainties, suggesting that useful information from the satellite data is present.

The European Transcom region has uncertainties in the satellite data (seasonal averages of 7.6–10.0 ppb) that are of comparable magnitude to the $\mu_{\Delta XCH_4}$ values (8.1–10.7 ppb), especially when considering the combination of the a posteriori and model XCO_2 uncertainties. However, the standard deviation of the $\mu_{\Delta XCH_4}$ values is highly variable (8.7–13.2 ppb) which suggests that there is scope for the observational data to aid in constraining the European XCH_4 fluxes.

Finally, the Australian Transcom region shows very small uncertainties in the satellite data. The uncertainty associated with the model XCO_2 is comparable to the a posteriori error during the Australian spring months but even in those circumstances, the $\mu_{\Delta XCH_4}$ values are far larger (11.4 ppb vs. 4.7 ppb), demonstrating that the satellite data are capable of providing some information to the inversion over Australia, although this may be limited in its ability to provide specific information on Australian sources as the $\sigma_{\Delta XCH_4}$ values over this region are similar to the estimated uncertainties with seasonal averages of 4.5–5.2 ppb compared to the total uncertainty values of 4.1–5.0 ppb.

6 Summary and conclusions

We present details of the update to the University of Leicester GOSAT Proxy XCH_4 v5.0 data set with 5 years of GOSAT data now processed. The data are validated against the latest ground-based TCCON data and found to agree well with on average a small bias of 4.8 ppb (~ 0.27 %), a single-sounding precision of 13.4 ppb (~ 0.74 %), and a relative accuracy of 4.2 ppb. For the first time the XCH_4 / XCO_2 ratio component of the proxy retrieval is validated and also found to agree well with TCCON with a bias of 0.014 ppb ppm^{-1} (~ 0.3 %) and a single-sounding precision of 0.033 ppb ppm^{-1} (~ 0.72 %).

A major unknown uncertainty in previous Proxy XCH_4 products was the uncertainty associated with the model XCO_2. In this work we validate three separate state-of-the-art chemistry transport models against the TCCON data and find that although the models can differ greatly (> 4 ppm) away from the TCCON stations, at the validation locations it is difficult to distinguish which model performs better from our comparisons. We therefore decide to use the median of the three models to act as the model XCO_2 in the calculation of the Proxy XCH_4 and use the maximum difference to the median as a measure of the uncertainty in the model XCO_2. This model uncertainty is found to vary greatly in time and space but is typically largest over regions associated with biomass burning such as central Africa and in particular over the Eurasian regions during summer months where large uptake in CO_2 leads to large differences between the models.

In order to assess the relative importance of these uncertainties, we compare this model XCO_2 uncertainty to the a posteriori retrieval error over the different Transcom regions and find typically that where there is seasonality in the uncertainties, it is typically directly out of phase between the two, resulting in the model XCO_2 uncertainty becoming significant during summer months where the a posteriori error is at its lowest. This relates to the fact that more sunlight leads to a reduction in the a posteriori uncertainty (by virtue of providing a greater signal in the SWIR) and at the same time is associated with an increase in photosynthesis and, hence, more potential for differences in the model XCO_2.

We assess the significance of these uncertainties on any flux inversion by comparing the mean and standard deviation of the GOSAT−MACC differences ($\mu_{\Delta XCH_4}$ and $\sigma_{\Delta XCH_4}$) to the estimated uncertainties. We find that for the majority of regions the mean and standard deviation of the ΔXCH_4 values are much larger than the estimated uncertainties, even taking into account the uncertainty related to the model XCO_2. Our findings show that useful information will be provided to the inversions for the majority of regions, with the exceptions being the boreal regions (North American Boreal and Eurasian Boreal) where the uncertainty is of a similar magnitude to the $\mu_{\Delta XCH_4}$ and $\sigma_{\Delta XCH_4}$ values. It is important to note that the MACC data are already constrained by NOAA background sites.

One final consideration for users of the Proxy XCH_4 data who are performing atmospheric inversions is that, should they have their own XCO_2 model which they believe is consistent with their XCH_4 model, it may be beneficial to only take the GOSAT XCH_4 / XCO_2 ratio and apply their own model XCO_2 (with appropriate averaging kernels) in order to minimise transport model errors between the different models. Alternatively the XCH_4 / XCO_2 ratio can also be inverted directly as shown in Fraser et al. (2014) and Pandey et al. (2015).

Appendix A: Data sets

The GOSAT Proxy XCH_4 data used in this publication are freely available from http://www.leos.le.ac.uk/GHG/ghg_cci/CRDP/data_2/ESACCI/GHG/GOSAT/CH4_GOS_OCPR/5.1/ upon request of a password. An updated version of this data set is now available (version 6.0) covering 2009–2014. Additionally, these data now contain both the raw XCH_4 and XCO_2 values as well as the uncertainty associated with the model XCO_2.

The TCCON XCH_4 and XCO_2 data used in this publication are publicly available from http://tccon.ornl.gov. The following data have been used: Sodankylä (Kivi et al., 2014), Bialystok (Deutscher et al., 2014), Karlsruhe (Hase et al., 2014), Orleans (Warneke et al., 2014), Garmisch (Sussmann and Rettinger, 2014), Park Falls (Wennberg et al., 2014a), Lamont (Wennberg et al., 2014b), Saga (Kawakami et al., 2014), Darwin (Griffith et al., 2014a), Wollongong (Griffith et al., 2014b), Lauder120 (Sherlock et al., 2014a), and Lauder125 (Sherlock et al., 2014b).

Table A1. Table showing the comparison statistics between each XCO_2 model (sampled as per the GOSAT measurements) within $\pm 2°$ of each TCCON site against the TCCON validation data. The difference (model−TCCON), the standard deviation of the difference, and the correlation coefficient are all provided as is the total number of measurements for each site, *N*, and the percentage "share" of the median for each model, %. For each of the three models, GEOS-Chem, MACC-II, and CarbonTracker, the best (bold) and worst (italic) value for each metric is highlighted. For the ensemble median data, all values which are better than the best individual model value are highlighted in bold-italic. The lower panel provides overall statistics across all sites. These include the relative accuracy (the standard deviation of the individual site biases), the overall precision (the standard deviation of the GOSAT−TCCON differences), and the overall share that each model contributes to the median ensemble.

$2° \times 2°$ Coincident criteria		GEOS-Chem				MACC-II				CarbonTracker				Ensemble median		
TCCON Site	*N*	Diff (ppm)	SD (ppm)	*r*	%	Diff (ppm)	SD (ppm)	*r*	%	Diff (ppm)	SD (ppm)	*r*	%	Diff (ppm)	SD (ppm)	*r*
Sodankylä	584	1.1	*1.1*	*0.97*	20	**0.9**	**0.9**	0.98	37	*1.2*	**0.9**	**0.99**	42	1.1	***0.8***	***0.99***
Bialystok	1429	*0.6*	*1.5*	*0.95*	25	**0.4**	1.1	0.97	33	*0.6*	**1.0**	**0.98**	44	0.6	***1.0***	0.97
Karlsruhe	1569	**−0.2**	*1.4*	*0.92*	22	*−0.6*	**1.1**	**0.95**	33	−0.4	**1.1**	**0.95**	45	−0.4	***1.1***	***0.95***
Orleans	1650	**0.3**	*1.2*	*0.95*	22	**0.3**	**0.9**	**0.98**	33	*0.4*	**0.9**	0.97	46	***0.3***	***0.8***	***0.98***
Garmisch	1527	*0.8*	*1.3*	*0.93*	22	**0.6**	*1.3*	0.94	34	*0.8*	**1.2**	**0.95**	43	0.7	***1.1***	***0.95***
Park Falls	2434	0.4	*1.1*	*0.97*	23	**0.1**	**1.0**	**0.98**	38	*0.5*	**1.0**	**0.98**	40	0.3	***0.9***	***0.98***
Lamont	7464	*−0.2*	*1.6*	*0.92*	20	−0.1	**0.9**	**0.98**	39	**0.0**	**0.9**	**0.98**	41	−0.1	***0.9***	***0.98***
Saga	379	−0.6	*1.1*	*0.93*	27	*−1.0*	**0.9**	**0.95**	33	**−0.3**	**0.9**	**0.95**	40	−0.6	***0.9***	***0.96***
Darwin	2491	**0.0**	*0.8*	*0.97*	12	*0.5*	0.7	*0.97*	27	0.4	**0.6**	**0.98**	60	0.3	***0.6***	***0.98***
Wollongong	2601	**−0.1**	**0.8**	**0.96**	36	**−0.1**	**0.8**	**0.96**	44	*0.2*	*0.9*	*0.95*	21	***0.0***	***0.8***	***0.96***
Lauder_120	124	**−0.1**	*0.9*	*0.82*	27	*−0.3*	**0.7**	**0.86**	44	−0.2	0.8	0.84	29	−0.2	0.8	0.84
Lauder_125	368	0.3	*0.4*	**0.99**	30	**0.2**	**0.3**	**0.99**	40	*0.4*	*0.4*	**0.99**	30	0.3	***0.3***	***0.99***
Statistics for all sites																
Relative accuracy (ppm)		0.48				0.53				0.47				0.48		
Overall precision (ppm)		1.3				0.97				0.96				0.92		
Total median share (%)		22				36				41						

Table A2. Table showing the seasonal averages of the data plotted in Fig. 7 for each of the Transcom regions. The retrieved a posteriori error, the uncertainty related to the model XCO_2, their combined total, and the mean and standard deviation of the GOSAT−MACC difference are all provided for each season and for each Transcom region.

Region	Season	A posteriori (ppb)	Model (ppb)	Total (ppb)	$\mu_{\Delta XCH_4}$ (ppb)	$\sigma_{\Delta XCH_4}$ (ppb)	Region	Season	A posteriori (ppb)	Model (ppb)	Total (ppb)	$\mu_{\Delta XCH_4}$ (ppb)	$\sigma_{\Delta XCH_4}$ (ppb)
North America boreal	spring	7.4	2.2	7.8	6.3	13.0	Eurasian boreal	spring	7.1	3.2	8.0	4.5	13.1
	summer	6.6	4.9	8.3	2.9	9.6		summer	6.3	7.0	9.5	4.4	9.9
	autumn	10.0	2.8	10.5	6.2	11.4		autumn	9.0	3.1	9.6	5.4	11.1
	winter	10.8	2.3	11.1	11.5	14.5		winter	9.9	2.5	10.3	5.7	13.9
North America temperate	spring	5.1	3.0	6.0	11.2	9.2	Eurasian temperate	spring	4.4	3.5	5.7	11.7	9.7
	summer	4.6	4.7	6.6	7.4	8.6		summer	4.3	5.8	7.3	5.5	15.0
	autumn	5.3	3.1	6.3	7.7	8.4		autumn	4.4	4.1	6.2	6.5	10.2
	winter	6.5	2.4	6.9	11.6	10.0		winter	5.2	2.6	5.8	9.9	9.6
South America tropical	spring	6.4	4.3	7.8	8.6	11.2	Tropical Asia	spring	6.0	6.0	8.5	8.9	12.2
	summer	5.3	4.3	6.9	10.8	8.6		summer	6.9	5.0	8.7	10.9	16.1
	autumn	5.8	5.2	7.9	10.7	12.6		autumn	6.2	6.0	8.7	11.7	16.8
	winter	6.5	4.1	7.8	7.4	15.5		winter	5.6	4.4	7.2	10.9	9.0
South America temperate	spring	4.7	3.7	6.1	6.0	10.7	Australia	spring	3.9	2.5	4.7	11.4	4.7
	summer	4.3	3.4	5.5	9.1	7.4		summer	3.7	1.8	4.1	11.7	4.5
	autumn	4.2	3.7	5.7	9.1	9.7		autumn	3.7	2.1	4.3	13.9	5.2
	winter	4.7	3.8	6.1	7.2	13.5		winter	4.2	2.5	5.0	15.0	5.2
Northern Africa	spring	3.6	3.6	5.2	8.8	7.3	Europe	spring	6.7	3.5	7.6	9.2	12.1
	summer	3.6	4.6	5.9	7.2	7.4		summer	5.9	5.3	8.0	10.7	8.7
	autumn	3.4	3.5	4.9	12.3	8.4		autumn	7.5	3.0	8.2	8.1	8.9
	winter	3.3	2.8	4.3	8.0	4.9		winter	9.4	3.1	10.0	9.3	13.2
Southern Africa	spring	4.7	4.6	6.7	15.5	9.9							
	summer	3.7	3.4	5.1	12.6	5.7							
	autumn	4.8	3.7	6.1	13.5	9.8							
	winter	5.4	4.8	7.3	19.8	10.7							

Acknowledgements. We thank Japanese Aerospace Exploration Agency, National Institute for Environmental Studies, and the Ministry of Environment for the GOSAT data and their continuous support as part of the Joint Research Agreement. R. J. Parker is funded through an ESA Living Planet Fellowship. The work at the University of Leicester and University of Edinburgh was supported by funding through the UK National Centre for Earth Observation (NCEO), the Natural Environment Research Council (NERC), and the ESA Greenhouse Gas Climate Change Initiative (GHG-CCI). Part of this work was funded by the NERC Amazonian Carbon Observatory project (NE/J016284/1) and the NERC GAUGE project (NE/K002465/1). This research used the ALICE High Performance Computing Facility at the University of Leicester.

The authors would like to thank Paul Wennberg as the TCCON PI for provision of TCCON data. The European TCCON groups acknowledge financial support by the EU project InGOS. The RAMCES team at LSCE (Gif-sur-Yvette, France) is acknowledged for maintenance and logistical work for the Orléans TCCON site. The University of Bremen acknowledges support from the Senate of Bremen, the EU-project ICOS-INWIRE, and operational funding from the National Institute for Environmental Studies (NIES, Japan). A part of the work at JAXA was supported by the Environment Research and Technology Development Fund (A-1102) of the Ministry of the Environment, Japan. A part of this work has been supported by the European Commission Seventh Framework Programme (FP7/2007–2013) projects MACC under grant agreement 218793 and MACC-II under grant agreement 283576.

Edited by: I. Aben

References

Alexe, M., Bergamaschi, P., Segers, A., Detmers, R., Butz, A., Hasekamp, O., Guerlet, S., Parker, R., Boesch, H., Frankenberg, C., Scheepmaker, R. A., Dlugokencky, E., Sweeney, C., Wofsy, S. C., and Kort, E. A.: Inverse modelling of CH_4 emissions for 2010–2011 using different satellite retrieval products from GOSAT and SCIAMACHY, Atmos. Chem. Phys., 15, 113–133, doi:10.5194/acp-15-113-2015, 2015.

Bergamaschi, P., Frankenberg, C., Meirink, J. F., Krol, M., Dentener, F., Wagner, T., Platt, U., Kaplan, J. O., Korner, S., Heinmann, M., Dlugokencky, E. J., and Goede, A.: Satellite chartography of atmospheric methane from SCIAMACHY on board ENVISAT: 2. Evaluation based on inverse model simulations, J. Geophys. Res.-Atmos., 112, D02304 doi:10.1029/2005JD006235, 2007.

Bergamaschi, P., Frankenberg, C., Meirink, J. F., Krol, M., Villani, M. G., Houweling, S., Frank, D., Edward, J. D., John, B. M., Luciana, V. G., Andreas, E., and Ingeborg, L.: Inverse modeling of global and regional CH_4 emissions using SCIAMACHY satellite retrievals, J. Geophys. Res.-Atmos., 114, D22301, doi:10.1029/2009JD012287, 2009.

Bergamaschi, P., Houweling, S., Segers, A., Krol, M., Frankenberg, C., Scheepmaker, R. A., Dlugokencky, E., Wofsy, S. C., Kort, E. A., Sweeney, C., Schuck, T., Brenninkmeijer, C., Chen, H., Beck, V., and Gerbig, C.: Atmospheric CH_4 in the first decade of the 21st century: inverse modeling analysis using SCIAMACHY satellite retrievals and NOAA surface measurements, J. Geophys. Res.-Atmos., 118, 7350–7369, doi:10.1002/jgrd.50480, 2013.

Boesch, H., Baker, D., Connor, B., Crisp, D., and Miller, C.: Global characterization of CO_2 column retrievals from shortwave-infrared satellite observations of the Orbiting Carbon Observatory-2 Mission, Remote Sensing, 3, 270–304, doi:10.3390/rs3020270, 2011.

Bousquet, P., Ciais, P., Miller, J. B., Dlugokencky, E. J., Hauglustaine, D. A., Prigent, C., Van Der Werf, G. R., Peylin, P., Brunke, E., Carouge, C., Langenfelds, R. L., Lathiere, J., Papa, F., Ramonet, M., Schmidt, M., Steele, L. P., Tyler, S. C., and White, J.: Contribution of anthropogenic and natural sources to atmospheric methane variability, Nature, 443, 439–443, doi:10.1038/nature05132, 2006.

Buchwitz, M., Reuter, M., Schneising, O., Boesch, H., Guerlet, S., Dils, B., Aben, I., Armante, R., Bergamaschi, P., Blumenstock, T., Bovensmann, H., Brunner, D., Buchmann, B., Burrows, J., Butz, A., Chedin, A., Chevallier, F., Crevoisier, C., Deutscher, N., Frankenberg, C., Hase, F., Hasekamp, O., Heymann, J., Kaminski, T., Laeng, A., Lichtenberg, G., Maziere, M. D., Noel, S., Notholt, J., Orphal, J., Popp, C., Parker, R., Scholze, M., Sussmann, R., Stiller, G., Warneke, T., Zehner, C., Bril, A., Crisp, D., Griffith, D., Kuze, A., O'Dell, C., Oshchepkov, S., Sherlock, V., Suto, H., Wennberg, P., Wunch, D., Yokota, T., and Yoshida, Y.: The Greenhouse Gas Climate Change Initiative (GHG-CCI): comparison and quality assessment of near-surface-sensitive satellite-derived CO_2 and CH_4 global data sets, Remote Sens. Environ., 162, 344–362, doi:10.1016/j.rse.2013.04.024, 2013.

Butz, A., Hasekamp, O. P., Frankenberg, C., Vidot, J., and Aben, I.: CH_4 retrievals from space-based solar backscatter measurements: performance evaluation against simulated aerosol and cirrus loaded scenes, J. Geophys. Res.-Atmos., 115, D24302, doi:10.1029/2010JD014514, 2010.

Chevallier, F., Ciais, P., Conway, T., Aalto, T., Anderson, B., Bousquet, P., Brunke, E., Ciattaglia, L., Esaki, Y., Fröhlich, M., Gomez, A., Gomez-Pelaez, A., Haszpra, L., Krummel, P., Langenfelds, R., Leuenberger, M., MacHida, T., Maignan, F., Matsueda, H., Morguí, J., Mukai, H., Nakazawa, T., Peylin, P., Ramonet, M., Rivier, L., Sawa, Y., Schmidt, M., Steele, L., Vay, S., Vermeulen, A., Wofsy, S., and Worthy, D.: CO_2 surface fluxes at grid point scale estimated from a global 21 year reanalysis of atmospheric measurements, J. Geophys. Res.-Atmos., 115, D21307, doi:10.1029/2010JD013887, 2010.

Chipperfield, M. P.: Multiannual simulations with a three-dimensional chemical transport model, J. Geophys. Res.-Atmos., 104, 1781–1805, doi:10.1029/98JD02597, 1999.

Cogan, A., Boesch, H., Parker, R., Feng, L., Palmer, P., Blavier, J.-F., Deutscher, N. M., Macatangay, R., Notholt, J., Roehl, C., Warneke, T., and Wunch, D.: Atmospheric carbon dioxide retrieved from the Greenhouse gases Observing SATellite (GOSAT): comparison with ground-based TCCON observations and GEOS-Chem model calculations, J. Geophys. Res.-Atmos., 117, D21301, doi:10.1029/2012JD018087, 2012.

Connor, B. J., Boesch, H., Toon, G., Sen, B., Miller, C., and Crisp, D.: Orbiting Carbon Observatory: inverse method and prospective error analysis, J. Geophys. Res.-Atmos., 113, D05305, doi:10.1029/2006JD008336, 2008.

Cressot, C., Chevallier, F., Bousquet, P., Crevoisier, C., Dlugokencky, E. J., Fortems-Cheiney, A., Frankenberg, C., Parker, R., Pison, I., Scheepmaker, R. A., Montzka, S. A., Krummel, P. B., Steele, L. P., and Langenfelds, R. L.: On the consistency between global and regional methane emissions inferred from SCIAMACHY, TANSO-FTS, IASI and surface measurements, Atmos. Chem. Phys., 14, 577–592, doi:10.5194/acp-14-577-2014, 2014.

Dee, D. P., Uppala, S. M., Simmons, A. J., Berrisford, P., Poli, P., Kobayashi, S., Andrae, U., Balmaseda, M. A., Balsamo, G., Bauer, P., Bechtold, P., Beljaars, A. C. M., van de Berg, L., Bidlot, J., Bormann, N., Delsol, C., Dragani, R., Fuentes, M., Geer, A. J., Haimberger, L., Healy, S. B., Hersbach, H., Hólm, E. V., Isaksen, L., Kållberg, P., Köhler, M., Matricardi, M., McNally, A. P., Monge-Sanz, B. M., Morcrette, J.-J., Park, B.-K., Peubey, C., de Rosnay, P., Tavolato, C., Thépaut, J.-N., and Vitart, F.: The ERA-Interim reanalysis: configuration and performance of the data assimilation system, Q. J. Roy. Meteor. Soc., 137, 553–597, doi:10.1002/qj.828, 2011.

Deutscher, N., Notholt, J., Messerschmidt, J., Weinzierl, C., Warneke, T., Petri, C., Grupe, P., and Katrynski, K.: TCCON Data Archive, hosted by the Carbon Dioxide Information Analysis Center, Oak Ridge National Laboratory, Oak Ridge, Tennessee, USA, doi:10.14291/tccon.ggg2014.bialystok01.R0/1149277, 2014.

Dils, B., Buchwitz, M., Reuter, M., Schneising, O., Boesch, H., Parker, R., Guerlet, S., Aben, I., Blumenstock, T., Burrows, J. P., Butz, A., Deutscher, N. M., Frankenberg, C., Hase, F., Hasekamp, O. P., Heymann, J., De Mazière, M., Notholt, J., Sussmann, R., Warneke, T., Griffith, D., Sherlock, V., and Wunch, D.: The Greenhouse Gas Climate Change Initiative (GHG-CCI): comparative validation of GHG-CCI SCIAMACHY/ENVISAT and TANSO-FTS/GOSAT CO_2 and CH_4 retrieval algorithm products with measurements from the TCCON, Atmos. Meas. Tech., 7, 1723–1744, doi:10.5194/amt-7-1723-2014, 2014.

Dlugokencky, E. J., Bruhwiler, L., White, J. W. C., Emmons, L. K., Novelli, P. C., Montzka, S. A., Masarie, K. A., Lang, P. M., Crotwell, A. M., Miller, J. B., and Gatti, L. V.: Observational constraints on recent increases in the atmospheric CH_4 burden, Geophys. Res. Lett., 36, L18803, doi:10.1029/2009GL039780, 2009.

Feng, L., Palmer, P. I., Yang, Y., Yantosca, R. M., Kawa, S. R., Paris, J.-D., Matsueda, H., and Machida, T.: Evaluating a 3-D transport model of atmospheric CO_2 using ground-based, aircraft, and space-borne data, Atmos. Chem. Phys., 11, 2789–2803, doi:10.5194/acp-11-2789-2011, 2011.

Frankenberg, C., Meirink, J. F., Bergamaschi, P., Goede, A. P. H., Heimann, M., Körner, S., Platt, U., van Weele, M., and Wagner, T.: Satellite chartography of atmospheric methane from SCIAMACHY on board ENVISAT: analysis of the years 2003 and 2004, J. Geophys. Res.-Atmos., 111, D07303, doi:10.1029/2005JD006235, 2006.

Frankenberg, C., Aben, I., Bergamaschi, P., Dlugokencky, E., Van Hees, R., Houweling, S., Van Der Meer, P., Snel, R., and Tol, P.: Global column-averaged methane mixing ratios from 2003 to 2009 as derived from SCIAMACHY: trends and variability, J. Geophys. Res.-Atmos., 116, D04302, doi:10.1029/2010JD014849, 2011.

Fraser, A., Palmer, P. I., Feng, L., Boesch, H., Cogan, A., Parker, R., Dlugokencky, E. J., Fraser, P. J., Krummel, P. B., Langenfelds, R. L., O'Doherty, S., Prinn, R. G., Steele, L. P., van der Schoot, M., and Weiss, R. F.: Estimating regional methane surface fluxes: the relative importance of surface and GOSAT mole fraction measurements, Atmos. Chem. Phys., 13, 5697–5713, doi:10.5194/acp-13-5697-2013, 2013.

Fraser, A., Palmer, P. I., Feng, L., Bösch, H., Parker, R., Dlugokencky, E. J., Krummel, P. B., and Langenfelds, R. L.: Estimating regional fluxes of CO2 and CH_4 using space-borne observations of XCH_4: XCO_2, Atmos. Chem. Phys., 14, 12883–12895, doi:10.5194/acp-14-12883-2014, 2014.

Griffith, D. W. T., Deutscher, N., Velazco, V. A., Wennberg, P. O., Yavin, Y., Aleks, G. K., Washenfelder, R., Toon, G. C., Blavier, J.-F., Murphy, C., Jones, N., Kettlewell, G., Connor, B., Macatangay, R., Roehl, C., Ryczek, M., Glowacki, J., Culgan, T., and Bryant, G.: TCCON Data from Darwin, Australia, Release GGG2014R0. TCCON Data Archive, hosted by the Carbon Dioxide Information Analysis Center, Oak Ridge National Laboratory, Oak Ridge, Tennessee, USA, doi:10.14291/tccon.ggg2014.darwin01.R0/1149290, 2014a.

Griffith, D. W. T., Velazco, V. A., Deutscher, N., Murphy, C., Jones, N., Wilson, S., Macatangay, R., Kettlewell, G., Buchholz, R. R., and Riggenbach, M.: TCCON Data from Wollongong, Australia, Release GGG2014R0. TCCON Data Archive, hosted by the Carbon Dioxide Information Analysis Center, Oak Ridge National Laboratory, Oak Ridge, Tennessee, USA, doi:10.14291/tccon.ggg2014.wollongong01.R0/1149291, 2014b.

Gurney, K., Law, R., Denning, A., Rayner, P., Baker, D., Bousquet, P., Bruhwiler, L., Chen, Y.-H., Clals, P., Fan, S., Fung, I., Gloor, M., Heimann, M., Higuchi, K., John, J., Maki, T., Maksyutov, S., Masarie, K., Peylin, P., Prather, M., Pak, B., Randerson, J., Sarmiento, J., Taguchi, S., Takahashi, T., and Yuen, C.-W.: Towards robust regional estimates of CO_2 sources and sinks using atmospheric transport models, Nature, 415, 626–630, doi:10.1038/415626a, 2002.

Hase, F., Blumenstock, T., Dohe, S., Grofl, J., and Kiel, M.: TCCON Data from Karlsruhe, Germany, Release GGG2014R0, TCCON Data Archive, hosted by the Carbon Dioxide Information Analysis Center, Oak Ridge National Laboratory, Oak Ridge, Tennessee, USA, doi:10.14291/tccon.ggg2014.karlsruhe01.R0/1149270, 2014.

Houweling, S., Krol, M., Bergamaschi, P., Frankenberg, C., Dlugokencky, E. J., Morino, I., Notholt, J., Sherlock, V., Wunch, D., Beck, V., Gerbig, C., Chen, H., Kort, E. A., Röckmann, T., and Aben, I.: A multi-year methane inversion using SCIAMACHY, accounting for systematic errors using TCCON measurements, Atmos. Chem. Phys., 14, 3991–4012, doi:10.5194/acp-14-3991-2014, 2014.

Kawakami, S., Ohyama, H., Arai, K., Okumura, H., Taura, C., Fukamachi, T., and Sakashita, M.: TCCON Data from Saga, Japan, Release GGG2014R0. TCCON Data Archive, hosted by the Carbon Dioxide Information Analysis Center, Oak Ridge National Laboratory, Oak Ridge, Tennessee, USA, doi:10.14291/tccon.ggg2014.saga01.R0/1149283, 2014.

Kirschke, S., Bousquet, P., Ciais, P., Saunois, M., Canadell, J. G., Dlugokencky, E. J., Bergamaschi, P., Bergmann, D., Blake, D. R., Bruhwiler, L., Cameron-Smith, P., Castaldi, S., Chevallier, F., Feng, L., Fraser, A., Heimann, M., Hodson, E. L., Houweling, S., Josse, B., Fraser, P. J., Krummel, P. B., Lamarque, J.-

F., Langenfelds, R. L., Le Quere, C., Naik, V., O'Doherty, S., Palmer, P. I., Pison, I., Plummer, D., Poulter, B., Prinn, R. G., Rigby, M., Ringeval, B., Santini, M., Schmidt, M., Shindell, D. T., Simpson, I. J., Spahni, R., Steele, L. P., Strode, S. A., Sudo, K., Szopa, S., van der Werf, G. R., Voulgarakis, A., van Weele, M., Weiss, R. F., Williams, J. E., and Zeng, G.: Three decades of global methane sources and sinks, Nat. Geosci., 6, 813–823, doi:10.1038/ngeo1955, 2013.

Kivi, R., Heikkinen, P., and Kyro., E.: TCCON Data from Sodankyla, Finland, Release GGG2014R0. TCCON Data Archive, hosted by the Carbon Dioxide Information Analysis Center, Oak Ridge National Laboratory, Oak Ridge, Tennessee, USA, doi:10.14291/tccon.ggg2014.sodankyla01.R0/1149280, 2014.

Kuze, A., Taylor, T., Kataoka, F., Bruegge, C., Crisp, D., Harada, M., Helmlinger, M., Inoue, M., Kawakami, S., Kikuchi, N., Mitomi, Y., Murooka, J., Naitoh, M., O'Brien, D., O'Dell, C., Ohyama, H., Pollock, H., Schwandner, F., Shiomi, K., Suto, H., Takeda, T., Tanaka, T., Urabe, T., Yokota, T., and Yoshida, Y.: Long-term vicarious calibration of GOSAT short-wave sensors: techniques for error reduction and new estimates of radiometric degradation factors, IEEE T. Geosci. Remote, 52, 3991–4004, doi:10.1109/TGRS.2013.2278696, 2014.

Messerschmidt, J., Macatangay, R., Notholt, J., Petri, C., Warneke, T., and Weinzierl, C.: Side by side measurements of CO_2 by ground-based Fourier transform spectrometry (FTS), Tellus B, 62, 749–758, doi:10.1111/j.1600-0889.2010.00491.x, 2010.

Monteil, G., Houweling, S., Butz, A., Guerlet, S., Schepers, D., Hasekamp, O., Frankenberg, C., Scheepmaker, R., Aben, I., and Röckmann, T.: Comparison of CH_4 inversions based on 15 months of GOSAT and SCIAMACHY observations, J. Geophys. Res.-Atmos., 118, 11807–11823, doi:10.1002/2013JD019760, 2013.

Myhre, G., Shindell, D., Bréon, F.-M., Collins, W., Fuglestvedt, J., Huang, J., Koch, D., Lamarque, J.-F., Lee, D., Mendoza, B., Nakajima, T., Robock, A., Stephens, G., Takemura, T., and Zhang, H.: Anthropogenic and natural radiative forcing, chap. 8, in: Climate Change 2013: the Physical Science Basis, Contribution of Working Group I to the Fifth Assessment Report of the Intergovernmental Panel on Climate Change, edited by: Stocker, T., Qin, D., Plattner, G.-K., Tignor, M., Allen, S., Boschung, J., Nauels, A., Xia, Y., Bex, V., and Midgley, P., Cambridge University Press, 659–740, doi:10.1017/CBO9781107415324.018, 2013.

Nisbet, E., Dlugokencky, E., and Bousquet, P.: Methane on the rise – again, Science, 343, 493–495, doi:10.1126/science.1247828, 2014.

O'Dell, C. W., Connor, B., Bösch, H., O'Brien, D., Frankenberg, C., Castano, R., Christi, M., Eldering, D., Fisher, B., Gunson, M., McDuffie, J., Miller, C. E., Natraj, V., Oyafuso, F., Polonsky, I., Smyth, M., Taylor, T., Toon, G. C., Wennberg, P. O., and Wunch, D.: The ACOS CO_2 retrieval algorithm – Part 1: Description and validation against synthetic observations, Atmos. Meas. Tech., 5, 99–121, doi:10.5194/amt-5-99-2012, 2012.

Pandey, S., Houweling, S., Krol, M., Aben, I., and Röckmann, T.: On the use of satellite-derived $CH_4 : CO_2$ columns in a joint inversion of CH4 and CO_2 fluxes, Atmos. Chem. Phys., 15, 8615–8629, doi:10.5194/acp-15-8615-2015, 2015.

Parker, R., Boesch, H., Cogan, A., Fraser, A., Feng, L., Palmer, P. I., Messerschmidt, J., Deutscher, N., Griffith, D. W. T., Notholt, J., Wennberg, P. O., and Wunch, D.: Methane observations from the Greenhouse Gases Observing SATellite: comparison to ground-based TCCON data and model calculations, Geophys. Res. Lett., 38, L15807, doi:10.1029/2011GL047871, 2011.

Peters, W., Jacobson, A. R., Sweeney, C., Andrews, A. E., Conway, T. J., Masarie, K., Miller, J. B., Bruhwiler, L. M. P., Petron, G., Hirsch, A. I., Worthy, D. E. J., Van Der Werf, G. R., Randerson, J. T., Wennberg, P. O., Krol, M. C., and Tans, P. P.: An atmospheric perspective on North American carbon dioxide exchange: CarbonTracker, P. Natl. Acad. Sci. USA, 104, 18925–18930, doi:10.1073/pnas.0708986104, 2007.

Prather, M. J., Holmes, C. D., and Hsu, J.: Reactive greenhouse gas scenarios: systematic exploration of uncertainties and the role of atmospheric chemistry, Geophys. Res. Lett., 39, L09803, doi:10.1029/2012GL051440, 2012.

Rigby, M., Prinn, R. G., Fraser, P. J., Simmonds, P. G., Langenfelds, R. L., Huang, J., Cunnold, D. M., Steele, L. P., Krummel, P. B., Weiss, R. F., O'Doherty, S., Salameh, P. K., Wang, H. J., Harth, C. M., Muhle, J., and Porter, L. W.: Renewed growth of atmospheric methane, Geophys. Res. Lett., 35, L22805, doi:10.1029/2008GL036037, 2008.

Rodgers, C.: Inverse Methods for Atmospheric Sounding: Theory and Practice, World Scientific Publishing Co Pte Ltd, 2000.

Schepers, D., Guerlet, S., Butz, A., Landgraf, J., Frankenberg, C., Hasekamp, O., Blavier, J.-F., Deutscher, N. M., Griffith, D. W. T., Hase, F., Kyro, E., Morino, I., Sherlock, V., Sussmann, R., and Aben, I.: Methane retrievals from Greenhouse Gases Observing Satellite (GOSAT) shortwave infrared measurements: performance comparison of proxy and physics retrieval algorithms, J. Geophys. Res.-Atmos., 117, D10307, doi:10.1029/2012JD017549, 2012.

Schneising, O., Buchwitz, M., Reuter, M., Heymann, J., Bovensmann, H., and Burrows, J. P.: Long-term analysis of carbon dioxide and methane column-averaged mole fractions retrieved from SCIAMACHY, Atmos. Chem. Phys., 11, 2863–2880, doi:10.5194/acp-11-2863-2011, 2011.

Sherlock, V., Connor, B., Robinson, J., Shiona, H., Smale, D., and Pollard, D.: TCCON Data from Lauder, New Zealand, 120HR, Release GGG2014R0. TCCON Data Archive, hosted by the Carbon Dioxide Information Analysis Center, Oak Ridge National Laboratory, Oak Ridge, Tennessee, USA, doi:10.14291/tccon.ggg2014.lauder01.R0/1149293, 2014a.

Sherlock, V., Connor, B., Robinson, J., Shiona, H., Smale, D., and Pollard, D.: TCCON Data from Lauder, New Zealand, 125HR, Release GGG2014R0. TCCON Data Archive, hosted by the Carbon Dioxide Information Analysis Center, Oak Ridge National Laboratory, Oak Ridge, Tennessee, USA, doi:10.14291/tccon.ggg2014.lauder02.R0/1149298, 2014b.

Sussmann, R. and Rettinger, M.: TCCON Data from Garmisch, Germany, Release GGG2014R0. TCCON Data Archive, hosted by the Carbon Dioxide Information Analysis Center, Oak Ridge National Laboratory, Oak Ridge, Tennessee, USA, doi:10.14291/tccon.ggg2014.garmisch01.R0/1149299, 2014.

Warneke, T., Messerschmidt, J., Notholt, J., Weinzierl, C., Deutscher, N., Petri, C., Grupe, P., Vuillemin, C., Truong, F., Schmidt, M., Ramonet, M., and Parmentier, E.: TCCON Data from Orleans, France, Release

GGG2014R0. TCCON Data Archive, hosted by the Carbon Dioxide Information Analysis Center, Oak Ridge National Laboratory, Oak Ridge, Tennessee, USA, doi:10.14291/tccon.ggg2014.orleans01.R0/1149276, 2014.

Wennberg, P. O., Roehl, C., Wunch, D., Toon, G. C., Blavier, J.-F., Washenfelder, R., Keppel-Aleks, G., Allen, N., and Ayers, J.: TCCON Data from Park Falls, Wisconsin, USA, Release GGG2014R0. TCCON Data Archive, hosted by the Carbon Dioxide Information Analysis Center, Oak Ridge National Laboratory, Oak Ridge, Tennessee, USA, doi:10.14291/tccon.ggg2014.parkfalls01.R0/1149161, 2014a.

Wennberg, P. O., Wunch, D., Roehl, C., Blavier, J.-F., Toon, G. C., Allen, N., Dowell, P., Teske, K., Martin, C., and Martin, J.: TCCON Data from Lamont, Oklahoma, USA, Release GGG2014R0. TCCON Data Archive, hosted by the Carbon Dioxide Information Analysis Center, Oak Ridge National Laboratory, Oak Ridge, Tennessee, USA, doi:10.14291/tccon.ggg2014.lamont01.R0/1149159, 2014b.

Wunch, D., Toon, G. C., Wennberg, P. O., Wofsy, S. C., Stephens, B. B., Fischer, M. L., Uchino, O., Abshire, J. B., Bernath, P., Biraud, S. C., Blavier, J.-F. L., Boone, C., Bowman, K. P., Browell, E. V., Campos, T., Connor, B. J., Daube, B. C., Deutscher, N. M., Diao, M., Elkins, J. W., Gerbig, C., Gottlieb, E., Griffith, D. W. T., Hurst, D. F., Jiménez, R., Keppel-Aleks, G., Kort, E. A., Macatangay, R., Machida, T., Matsueda, H., Moore, F., Morino, I., Park, S., Robinson, J., Roehl, C. M., Sawa, Y., Sherlock, V., Sweeney, C., Tanaka, T., and Zondlo, M. A.: Calibration of the Total Carbon Column Observing Network using aircraft profile data, Atmos. Meas. Tech., 3, 1351–1362, doi:10.5194/amt-3-1351-2010, 2010.

Wunch, D., Toon, G. C., Blavier, J.-F. L., Washenfelder, R. A., Notholt, J., Connor, B. J., Griffith, D. W. T., Sherlock, V., and Wennberg., P. O.: The Total Carbon Column Observing Network, Philos. T. Roy. Soc. A, 369, 2087–2112, doi:10.1098/rsta.2010.0240, 2011a.

Wunch, D., Wennberg, P. O., Toon, G. C., Connor, B. J., Fisher, B., Osterman, G. B., Frankenberg, C., Mandrake, L., O'Dell, C., Ahonen, P., Biraud, S. C., Castano, R., Cressie, N., Crisp, D., Deutscher, N. M., Eldering, A., Fisher, M. L., Griffith, D. W. T., Gunson, M., Heikkinen, P., Keppel-Aleks, G., Kyrö, E., Lindenmaier, R., Macatangay, R., Mendonca, J., Messerschmidt, J., Miller, C. E., Morino, I., Notholt, J., Oyafuso, F. A., Rettinger, M., Robinson, J., Roehl, C. M., Salawitch, R. J., Sherlock, V., Strong, K., Sussmann, R., Tanaka, T., Thompson, D. R., Uchino, O., Warneke, T., and Wofsy, S. C.: A method for evaluating bias in global measurements of CO_2 total columns from space, Atmos. Chem. Phys., 11, 12317–12337, doi:10.5194/acp-11-12317-2011, 2011b.

Yokota, T., Yoshida, Y., Eguchi, N., Ota, Y., Tanaka, T., Watanabe, H., and Maksyutov, S.: Global concentrations of CO_2 and CH_4 retrieved from GOSAT: first preliminary results, SOLA, 5, 160–163, doi:10.2151/sola.2009-041, 2009.